Precambrian Research 401 (2024) 107278

Contents lists available at ScienceDirect

Precambrian Research

journal homepage: www.elsevier.com/locate/precamres

Estuaries house Earth's oldest known non-marine eukaryotes

Grace C. Nielson [a,b,*], Eva E. Stüeken [a], Anthony R. Prave [a]

[a] School of Earth & Environmental Sciences, University of St Andrews, St Andrews KY16 9TS, Scotland
[b] Envireau Water Ltd., Unit 16, Beta Centre, Stirling University Innovation Park, Stirling FK9 4NF, Scotland

ARTICLE INFO

Keywords:
Diabaig Formation
Sleat Group
Eukaryote habitats
Sulfur isotopes

ABSTRACT

Some of the oldest postulated non-marine eukaryotic microfossils occur in the 1.1–1.0 Ga Poll a'Mhuillt, Loch na Dal, and Diabaig formations in NW Scotland. These sedimentary strata have traditionally been interpreted as lacustrine. Here we report new trace element, sulfur isotope and metal abundance data and sedimentological observations for the latter two units. The geochemical data imply low salinity, oxic conditions whereas sedimentological features indicate marine tide and storm processes. Interpreting their depositional settings as estuaries, rather than lakes, with seawater-freshwater mixing fronts reconciles the contrasting datasets. Thus, whilst these microbial habitats likely experienced frequent seawater input, they appear to have experienced the lowest salinity conditions of all known *in situ* fossil assemblages in the Precambrian. The Torridonian may in fact be representative of the low-salinity habitats predicted for ancestral eukaryotes based on phylogenetic reconstructions. Estuarine settings with gradients in water chemistry over space and time may have facilitated the transition of eukaryotic life from land to sea.

1. Introduction

Organic-walled microfossils found in sedimentary units spanning the late Stenian through early Tonian have been highlighted as evidence for the earliest known colonisation of land by eukaryotes (e.g. Wellman & Strother, 2015). Three units central to that interpretation are the Poll a'Mhuillt, Loch na Dal, and Diabaig formations of the Stoer-Sleat-Torridon succession in northwest Scotland (Strother et al., 2011; Callow et al., 2011; Strother & Wellman, 2016,2021; Brasier et al., 2017). Existing age constraints place deposition of those strata to between c. 1.1 and 1.0 Ga (Krabbendam et al., 2022). Recent work suggested that the Poll a'Mhuillt sediments were likely deposited in marine-influenced rather than purely non-marine settings (Stüeken et al., 2017). Evidence for that includes pseudomorphs after gypsum, as well as enrichments in pyrite and molybdenum with isotopic characteristics consistent with Proterozoic seawater. A marine interpretation does not necessarily invalidate the inference of eukaryotic life on land at that time if the recovered organisms were transported to the depositional site by rivers (Strother et al., 2011). In fact, some prokaryotic microfossils of likely cyanobacterial affinity show strong resemblance to modern freshwater organisms while also displaying taphonomic evidence of riverine transport (Strother & Wellman, 2016). Careful characterization of the depositional environment is nevertheless important, because not all fossils are demonstrably allochthonous and therefore an incorrect interpretation may lead to incorrect conclusions about the habitat, nutrient availability, and physiological properties of these organisms. With that in mind, we revisited the depositional setting of the Diabaig and Loch na Dal formations.

These units are tens to several hundreds of metres thick and consist mostly of red-grey sandstone interbedded with varying proportions of grey mudstone; both comprise the lower part of the 4–6 km thick Sleat-Torridon succession of northwest Scotland (Krabbendam et al., 2022). The organic-walled microfossils recovered from those formations are typically preserved in dark greenish to greyish mudstones and in early diagenetic (pre-compaction) phosphate concretions (Strother et al., 2011). Historically, that succession has been interpreted as fluvial-lacustrine for two reasons (Stewart, 1988, 1991, 2002). First, illite separates from the mudstones display enrichments in boron, which Stewart & Parker (1979) interpreted as evidence of freshwater evaporation. Second, the mudstone-containing units are bounded by thick (hundreds of metres) sandstone bodies that are clearly of fluvial origin (e.g., Stewart, 2002; Ielpi & Ghinassi, 2015; McMahon & Davies, 2020). This association has led workers to infer that the mudstone units were also deposited in a lacustrine setting (Stewart, 2002 and references therein). However, a unit over- and under-lain by non-marine rocks is not necessarily itself non-marine. Further, the illite-boron proxy is not

* Corresponding author at: Envireau Water Ltd., Unit 16, Beta Centre, Stirling University Innovation Park, Stirling FK9 4NF, Scotland.
E-mail address: grace.c.nielson@gmail.com (G.C. Nielson).

https://doi.org/10.1016/j.precamres.2023.107278
Received 1 September 2023; Received in revised form 18 December 2023; Accepted 21 December 2023
Available online 2 January 2024

well calibrated, in particular for the Precambrian where little is known about aqueous boron reservoirs. To shed new light on the depositional setting of these strata, we re-examined the facies character of mudstone-dominated intervals in the Diabaig and Loch na Dal formations. In addition, we performed new geochemical analyses, including major and minor element abundances and sulfur isotope ratios.

2. Sampling and analytical methods

We studied both formations across the entirety of their outcrop belts, documented sedimentary features at outcrop scale, and chose six localities for geochemical sampling (Fig. 1). Thirty samples of dark grey shale from the Diabaig Formation and ten from the Loch na Dal Formation were collected for isotopic and elemental analyses (Tables 1 and 2) and prepared following standard protocols. The Diabaig localities sampled include the Type Locality (57.57756, –5.6861), Victoria Falls (57.679927, –5.533167), Ob Mheallaidh (57.531904, –5.612229), Raasay (57.44306, –6.02548), and Bagh na h-Uamha (56.994414, –6.247572) on the Isle of Rum. Because the Loch na Dal Formation in the lower Sleat Group also contains organic-walled microfossils (Strother et al., 2011) we sampled it at its Type Locality on Skye (57.16931, –5.77342). Samples were prepared and analysed in the geochemistry facilities at the University of St Andrews, Scotland. Hand samples were crushed into mm-sized chips using a hammer and steel plate and washed for 5–10 s by swirling in reagent grade methanol followed by 1 N HCl and, finally, 18.2 MΩ/cm DI-H_2O. After washing, the rock chips were

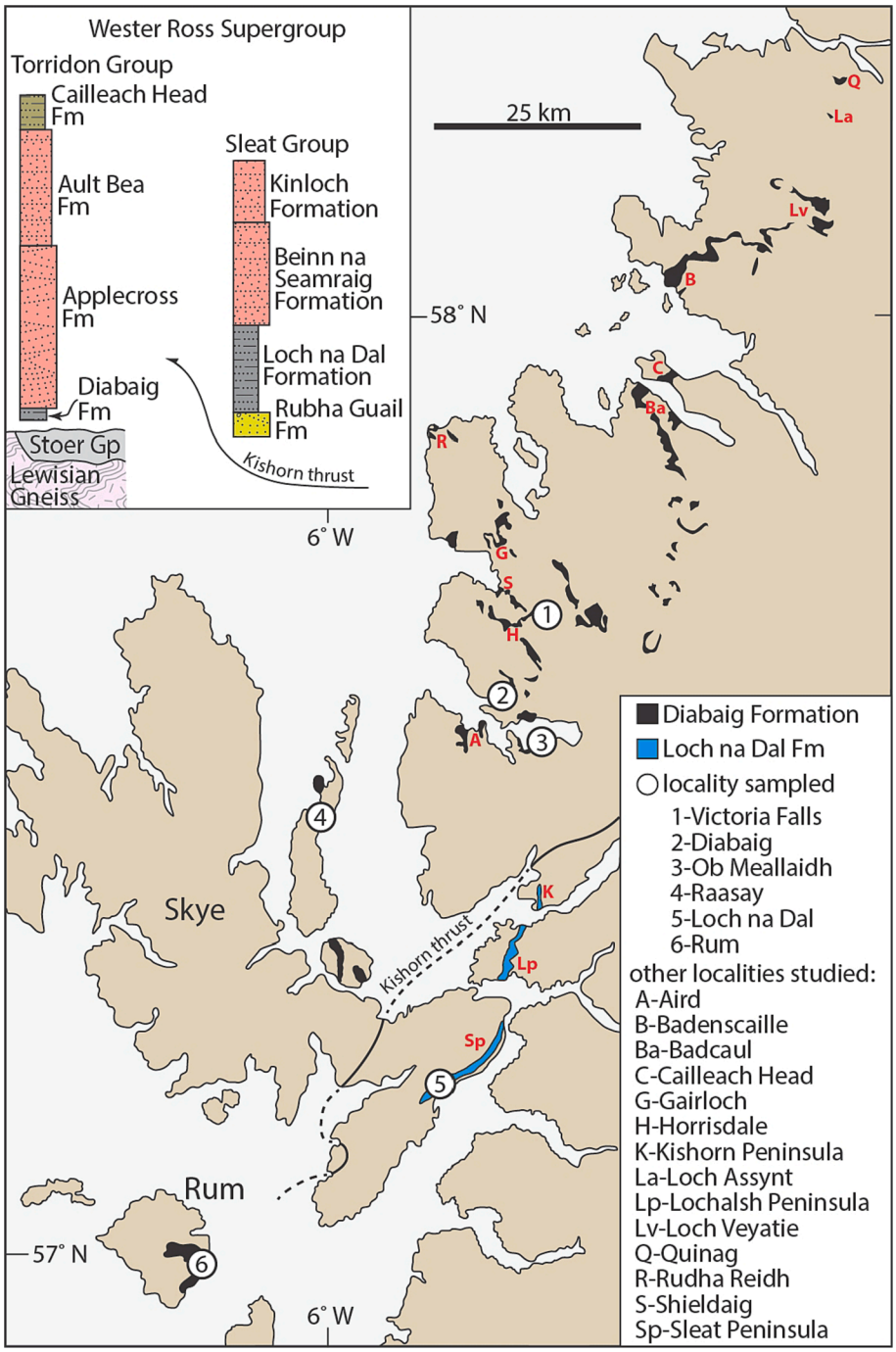

Fig. 1. Outcrop distribution of the Diabaig and Loch na Dal formations in NW Scotland.

Table 1
Carbon and sulfur data. TRS = total reduced sulfur, $\delta^{34}S_{bulk}$ = sulfur isotopes measured on decarbonated rock powders, $\delta^{34}S_{py}$ = sulfur isotopes measured on pyrite extracts, TOC = total organic carbon, $\delta^{13}C_{org}$ = organic carbon isotopes, S/C = ratio of TRS to TOC.

	TRS [μg/g]	$\delta^{34}S_{bulk}$ [‰]	$\delta^{34}S_{py}$ [‰]	TOC [%]	$\delta^{13}C_{org}$ [‰]	S/C [g/g]
Diabaig:						
Diabaig_180808-1	156	4.17	3.67	0.12	−30.54	0.13
Diabaig_180808-2	162	5.48	4.63	0.15	−31.40	0.11
Diabaig_180808-3	142	5.31	4.82	0.13	−30.53	0.11
Diabaig_180808-4	77	3.81	3.22	0.33	−29.74	0.02
Diabaig_180808-5	168	3.81	3.22	0.17	−30.59	0.10
Diabaig_180808-6	38	5.60		0.21	−30.03	0.02
Diabaig_180808-7	18	4.38		0.19	−30.11	0.01
Diabaig_180808-8	387	6.19	5.32	0.24	−30.63	0.16
Diabaig_180808-9	17			0.16	−30.41	0.01
Diabaig_180808-11	29	9.93		0.21	−29.99	0.01
Diabaig_180808-12	25	1.64		0.11	−30.05	0.02
Ob Meilleadh:						
Diabaig_180808-14	603	−0.32	−2.46	0.13	−27.13	0.46
Diabaig_180808-15	198	−1.73	−1.31	0.07	−30.38	0.28
Diabaig_180808-16	54	14.46		0.31	−27.97	0.02
Diabaig_180808-17	62	8.39	4.41	0.43	−28.53	0.01
Raasay:						
Diabaig_180809-1	47	6.71	4.93	0.08	−31.42	0.06
Diabaig_180809-2a	89	−13.90	−14.49	0.05	−30.74	0.17
Diabaig_180809-2b	72	0.84	1.44	0.09	−30.88	0.08
Diabaig_180809-3	62	4.14	2.75	0.10	−30.93	0.06
Victoria Falls:						
Victoria Falls 1A	216	−22.09	−25.73	0.43	−33.69	0.05
Victoria Falls 2A	30	−15.42		0.06	−30.18	0.05
Victoria Falls 3A	44	−13.91		0.16	−31.82	0.03
Victoria Falls 4A	39	−13.26		0.28	−31.84	0.01
Diabaig_180807-2	67	−15.68	−14.69	0.19	−31.39	0.04
Diabaig_180807-1	40	3.18		0.20	−31.07	0.02
Rum:						
Rum 1A	42	2.93	6.20	0.08	−28.29	0.05
Rum 2	116	4.07	12.24	0.09	−28.59	0.13
Rum 3A	184	5.78	6.90	0.09	−28.62	0.21
Rum 4A	45	2.59	3.98	0.10	−29.13	0.04
Rum 5A	44	2.07	4.23	0.10	−28.72	0.04
Sleat Group:						
Sleat TD	55	5.57	2.66	0.06	−31.26	0.10
Sleat_180809-4	91	4.19	4.94	0.15	−31.89	0.06
Sleat_180809-4	51	3.23		0.12	−29.27	0.04
Sleat_180809-6	130	3.51	2.77	0.09	−30.58	0.14
Sleat_180809-7	6			0.05	−28.85	0.01
Sleat_180809-8	38	0.48		0.13	−31.32	0.03
Sleat_180809-9	37	0.95	5.02	0.10	−28.69	0.04
Sleat_180809-10	53	1.99		0.14	−27.12	0.04
Sleat_180809-11	3			0.04	−28.29	0.01
Sleat_180809-12	94	3.13	3.10	0.11	−29.67	0.08

dried in a 60 ℃ oven overnight. The dry rock chips were then pulverised into a fine powder using an agate ball mill. Pre-combusted quartz sand (500 ℃ overnight) was run through the mill in between samples, and the final sample powders were stored in pre-combusted glass scintillation vials.

2.1. Trace metal analyses

Approximately 1 g of powder from each of the samples was sent to Australian Laboratory Services (ALS) in Dublin, Ireland, for whole-rock geochemical characterisation using their method ME-MS-61 of four-acid digestion (HCl, HNO_3, HF, $HClO_4$) followed by ICP-MS and -AES analyses. In addition, a subset of samples was submitted for total boron abundance measurements using NaOH fusion and ICP-MS analysis (ALS method B-MS82L). Reproducibility was assessed with rock standards OREAS-45d, OREAS-905 and MRGeo-08, and with sample replicates. It was found to be 5 % or better for all major elements and 4 % or better for all minor elements used in this study.

2.2. Organic carbon and sulfur isotope analyses

A separate aliquot of each powder was decarbonated for analyses of total organic carbon (TOC), organic carbon isotopes ($\delta^{13}C_{org}$), total reduced sulfur (TRS), and bulk reduced sulfur isotopes ($\delta^{34}S_{bulk}$). For the decarbonation, samples were weighed into pre-combusted (500 ℃) glass centrifuge tubes, mixed with 10 ml reagent grade 2 N HCl and left overnight at 60 ℃. The samples were centrifuged (700 rpm, 15 min) and the acid decanted. To test if samples were successfully decarbonated, a small amount of acid was added to ensure all carbonate had dissolved and there was no effervescence. Each sample was washed with 18.2 MΩ/cm DI–H_2O three times and left to dry at 60 ℃ for three days. Samples were transferred into pre-combusted scintillation vials for storage. This process removed all sulfate associated with carbonate and any potential traces of sulfur evaporite minerals such that remaining sulfur phases were organic- and pyrite-bound sulfide and elemental sulfur (these are referred to as TRS for total reduced sulfur).

2.3. Chromium reduction for pyrite extraction

To separate pyrite-bound (referred to as S_{py}) from organic-bound sulfur, the samples were subjected to chromium reduction (Canfield et al., 1986). First, 30 g of untreated rock powder were measured into 250 ml 2-neck round-bottom flasks (hereafter CR vessel). Approximately 10–20 ml of ethanol were used to rinse excess powder from the sides to the bottom of the vessel. The ethanol also aided in the reduction of elemental sulfur during the experiment if present. A magnetic stirrer was inserted into each flask that were then placed on hotplates at around 100 ℃ and flushed with N_2 gas. A 50 ml plastic centrifuge tube filled with 30 ml of 5 % Zn acetate solution (the H_2S trap) was attached to the outflow of the N_2 gas from each CR vessel, separated by a water-cooled condenser. Using a plastic syringe, 35 ml of $CrCl_2$ solution (in 0.5 M HCl) mixed with 15 ml of concentrated HCl was injected into each CR vessel. The $CrCl_2$ solution had been prepared from dissolved $CrCl_3$ by slow passage over Zn granules packed into a chromatography column. Upon reaction with the sample, the acidic $CrCl_2$ solution converted sulfide minerals into H_2S gas. The total amounts of sulfide in samples were so low that we did not perform a separate extraction of acid-volatile sulfur (AVS) using HCl alone. Once the Cr solution was added, the samples were allowed to react for two hours, during which N_2 gas carried the H_2S into the traps where it precipitated as white ZnS. After 2 h, 15 ml of 0.1 M $AgNO_3$ solution were added into each trap to convert the white ZnS into black Ag_2S. The flasks were centrifuged and the remaining solution decanted into a waste bottle. The Ag_2S samples were washed with DI-H_2O and centrifuged again. The DI-H_2O was decanted, and samples left to dry in a 60 C oven overnight. Twenty-six samples were processed successfully with the chromium reduction method;

Table 2
Major and minor elemental abundance data. Percentages are in weight percent. *This P measurement exceeded the detectable range and is provided as 1.5 times he upper limit.

	Al	B	Ba	Ca	Co	Cr	Cu	Fe	Ga	K	Mg	Mn	Mo	Na	Ni	P	Pb	Sr	Th	Ti	U	V	Zn
	[%]	[μg/g]	[μg/g]	[%]	[μg/g]	[μg/g]	[μg/g]	[%]	[μg/g]	[%]	[%]	[μg/g]	[μg/g]	[%]	[μg/g]	[%]	[μg/g]	[μg/g]	[μg/g]	[%]	[μg/g]	[μg/g]	[μg/g]
Diabaig																							
Diabaig_180808-1	7.88	35	590	0.7	21	53	47	4.76	22	2.56	1.22	535	0.5	1.43	41	0.03	15	114	11	0.45	4	83	121
Diabaig_180808-3	8.42	37	470	1.28	22	52	38	4.45	23	2.49	1.27	655	0.8	1.55	40	0.08	27	111	11	0.46	4	89	110
Diabaig_180808-5	8.93	32	550	0.78	24	72	65	5.11	26	2.87	1.51	606	0.6	1.34	49	0.07	19	105	12	0.54	5	109	132
Diabaig_180808-7	8.74	41	520	1.03	20	64	43	4.85	25	2.82	1.43	560	1.0	1.38	42	0.24	22	117	14	0.52	5	104	101
Diabaig_180808-9	8.73	59	690	1.43	21	61	9	4.72	25	3.31	1.39	527	0.6	1.36	40	0.44	14	142	14	0.51	5	101	111
Diabaig_180808-12	7.96	45	710	0.75	22	58	29	4.86	23	2.99	1.39	669	0.3	1.57	49	0.07	14	155	11	0.47	4	94	107
Ob Meilleadh																							
Diabaig_180808-14	7.52	25	710	1.35	22	82	40	4.31	22	2.47	1.07	680	0.6	2.44	45	0.04	76	277	7	0.52	3	111	99
Diabaig_180808-15	8.37	34	720	1.24	23	55	29	4.32	24	3.12	1.32	674	0.4	1.71	39	0.07	17	164	13	0.53	4	94	106
Diabaig_180808-16	7.84	30	880	2.76	23	86	24	4.95	25	2.89	1.18	701	1.3	1.68	51	0.78	16	241	12	0.55	5	126	111
Diabaig_180808-17	6.65	74	730	11.05	18	52	16	4.72	19	2.24	1.2	1210	4.5	1.36	41	1.50*	10	551	7	0.33	4	94	85
Raasay																							
Diabaig_180809-1	8.19	53	720	0.8	17	49	37	4.03	22	3.41	1.23	622	0.2	1.57	31	0.06	18	144	13	0.49	4	83	92
Diabaig_180809-2a	8.91	40	730	1.11	24	86	51	5.4	26	2.87	1.59	781	0.3	1.81	55	0.05	11	168	13	0.59	5	121	127
Diabaig_180809-2b	8.14	55	680	0.8	18	50	36	4.29	22	3.5	1.23	656	0.3	1.51	33	0.07	20	146	13	0.48	4	85	101
Diabaig_180809-3	8.44	55	730	0.83	18	50	40	4.41	23	3.6	1.29	672	0.3	1.53	34	0.07	21	151	13	0.49	4	86	103
Victoria Falls																							
Victoria Falls 1A	9.41	51	750	1.17	23	93	16	5.13	27	3.17	1.57	659	0.6	1.74	56	0.04	9	176	15	0.63	5	133	115
Victoria Falls 2A	8.10	54	770	0.87	23	84	27	4.91	27	3.34	1.33	551	0.1	1.51	59	0.03	8	138	10	0.57	5	127	125
Victoria Falls 3A	9.11	48	640	1.39	25	92	24	5.54	29	3.06	1.62	678	0.5	1.53	64	0.20	6	135	14	0.65	5	128	129
Victoria Falls 4A	8.94	47	760	2.26	20	73	12	4.63	27	3.14	1.32	554	0.7	1.50	47	0.65	20	166	14	0.52	6	112	106
Diabaig_180807-2	7.81	39	680	1.2	26	94	29	5.34	27	2.68	1.48	737	0.2	1.89	60	0.05	10	173	10	0.60	5	125	133
Diabaig_180807-1	8.77	36	570	1.16	21	67	35	4.75	25	2.67	1.22	483	0.9	1.50	53	0.25	14	142	11	0.49	4	104	107
Rum																							
R1A	9.04		860	0.31	21	62	44	4.91	26	4.23	1.42	529	0.3	1.17	41	0.07	17	82	11	0.53	4	113	108
R2	9.30		820	0.34	22	61	47	5.12	24	4.21	1.5	525	0.3	1.10	46	0.10	16	73	16	0.51	6	112	105
R3A	9.10		820	0.35	20	64	44	5.06	25	4.16	1.46	515	0.3	1.14	40	0.10	12	81	13	0.51	5	113	101
R4A	8.95		810	0.39	19	56	34	4.65	23	3.92	1.37	512	0.3	1.32	37	0.10	11	93	13	0.51	4	97	98
R5A	9.07		760	0.35	21	62	58	5.05	27	4.2	1.44	547	0.3	1.19	41	0.11	12	76	11	0.53	5	111	93
Sleat Group																							
Sleat Rum 190616–2	7.99		730	0.82	20	52	37	4.56	24	3.04	1.36	687	0.3	1.53	35	0.09	12	131	13	0.55	4	91	93
Sleat_180809-4	8.72		1070	1.71	31	113	66	5.6	31	3.8	1.58	855	0.4	1.76	64	0.15	19	236	15	0.87	7	163	142
Sleat_180809-12	8.78		930	1.42	29	81	64	5.17	28	2.99	1.76	715	1.2	2.48	48	0.32	17	195	11	0.58	5	127	132
Sleat_180809-6	7.74		970	1.28	29	80	57	5.33	27	3.12	1.51	743	0.5	2.02	55	0.07	10	272	9	0.57	4	115	120
Sleat_180809-9	8.60		870	0.81	21	60	42	4.72	25	3.37	1.4	601	0.6	1.20	40	0.07	17	70	13	0.54	5	103	105

sulfur content was too low in the other samples to obtain sufficient Ag_2S for analyses.

2.4. Carbon and sulfur isotope analysis

For organic carbon and bulk reduced sulfur isotopic analysis, including analyses of sulfur isotopes in the Ag_2S extracts, approximately 50 mg of each sample were mixed with 5–10 mg of V_2O_5 and weighed into tin capsules. The capsules were sealed and analysed by flash-combustion with an elemental analyser (EA Isolink) coupled to a continuous-flow isotope-ratio mass spectrometer (Thermo Fisher MAT253) via a Conflo IV. The combustion column of the EA was packed with WO_3 granules and electrolytic Cu wire held at 1020 C. This was followed by a water trap packed with magnesium perchlorate at room temperature. The oxygen pulse was set to 5 s at a flow of 250 ml/min. The flow of He gas, which carried the sample gas to the mass spectrometer, was decreased from 180 ml/min to 50 ml/min after 110 s to concentrate the SO_2 gas in the gas chromatography (GC) column. The GC oven of the EA was ramped-up from 35 ℃ to 240 ℃ during the run to improve elution and peak shape of CO_2 and SO_2. Analyses were calibrated to standard delta notation with USGS-40 and USGS-41 for carbon isotopes ($\delta^{13}C$ [‰] = $[(^{13}C/^{12}C)_{sample}/(^{13}C/^{12}C)_{VPDB} - 1]$ x 1000) and with IAEA-S2 and IAEA-S3 for sulfur isotopes ($\delta^{34}S$ [‰] = $[(^{34}S/^{32}S)_{sample}/(^{34}S/^{32}S)_{VCDT} - 1]$ x 1000). Peak areas of the standards were used to calibrate TOC and TRS abundances. Based on replicate analyses, analytical reproducibility (1SD) was 0.36 ‰ for $\delta^{13}C_{org}$ and 0.85 ‰ $\delta^{34}S_{bulk}$. For $\delta^{34}S_{py}$, we did not analyse sample replicates, but the reproducibility of standards of the same material was 0.11 ‰. The higher precision for $\delta^{34}S_{py}$ compared to $\delta^{34}S_{bulk}$ is attributed to the higher sulfur concentration in the former. The average reproducibility (relative error, RE) for total abundances was 5 % for TRS and 3 % for TOC.

3. Results

3.1. Sedimentary characteristics

Bed surfaces in both formations display evidence for shallow-water settings that experienced episodic exposure; these include desiccation cracks, short-wavelength, low-amplitude oscillation ripples, and microbially induced sedimentary structures such as *Kinneyia* and pustulose texture (e.g. Prave, 2002; Callow et al., 2011; Fig. 2). Evidence that those units were deposited by marine processes is the presence of flaser, lenticular, and pinstripe bedding, ripple foresets that are consistently outlined by mud drapes, ripple and cross-bed sets bounded by mud partings and containing multiple reactivation surfaces, wave, ladderback and combined-flow and flat-topped ripples, and, in many places, bimodal flow indicators such as herringbone cross-laminae and bimodal-opposed sets of migrating ripples (Fig. 3a–c). In places, conspicuous dm-thick sets of repetitively thicker-coarser and thinner-finer laminae bundles are developed (Fig. 3e–g). These features occur in every locality we examined across the Diabaig and Loch na Dal outcrop belts (Fig. 4) and are integral to a facies motif marked by thickening- and coarsening-upward as well as thinning- and fining-upward depositional cycles from a few metres to several tens of metres thick. The Type Locality of the Diabaig Formation in particular shows that the microfossil-bearing phosphatic nodules occur within sediment that contains ripples showing opposed migration directions (Fig. 5a–d). In the upper part of the Type Locality, sandstone beds display ball-and-pillow and soft-sediment deformation features and, in places, hummocky and swaley cross-stratification geometries marked by beds having flat bases and upward aggradational growth defined by low-angle convex and concave up laminae (Fig. 5e–g). The coarser and thicker bedded units consist of fine- to medium-grained quartzitic to feldspathic sandstone, most marked by low-angle parallel lamination and shallowly dipping trough cross-beds, rarely climbing ripples, and with bases that are either flat or have cm- to dm-scale erosive scalloping; in places m-scale channels are present (Fig. 6). Palaeocurrent data from these sandstones yield unidirectional sediment transport directions (ENE-directed; Stewart, 2002).

3.2. Elemental abundances and isotopic ratios

The geochemical data are summarised in Fig. 7 and Tables 1 and 2. Compositionally, the Diabaig and Loch na Dal formations are similar, but three samples have slightly higher than average Ca levels (>2 wt%) and show enrichment in Mo (up to 4.5 μg/g) and P (>0.5 wt%), and thus likely contain diagenetic phosphate (P concretions are present in both Diabaig and Loch na Dal strata; Stewart, 2002). Key elemental ratios (see below) yielded the following averages: Sr/Ba 0.20 ± 0.07, B/Ga 1.86 ± 0.65, Fe/Al 0.58 ± 0.05, U/Th 0.38 ± 0.06, Ni/Co 2.07 ± 0.25 and V/Cr 1.60 ± 0.15. The samples are lean in TOC and TRS, ranging from 0.04 to 0.43 wt% and 3 to 603 μg/g, respectively. C_{org}/P values range from 0.73 to 10.31 (excepting a sample from Victoria Falls with a C_{org}/P value of 27.72). Mass ratios of TRS/TOC range from 0.01 to 0.46 with a low median of 0.05. Values for $\delta^{13}C_{org}$ cluster between –33.7 ‰ and −27.1 ‰ and values for $\delta^{34}S_{bulk}$ and $\delta^{34}S_{py}$ range from –22.1 ‰ to + 14.5 ‰ and −25.7 ‰ to 12.2 ‰, respectively. $\delta^{34}S_{bulk}$ and $\delta^{34}S_{py}$ are well correlated ($r^2 = 0.90$), suggesting that we can use $\delta^{34}S_{bulk}$ to approximate the composition of pyrite where the chemical extraction of pyrite was not feasible.

4. Discussion

4.1. Sedimentary features indicative of tidal activity

The various sedimentary observations compiled and documented herein are most straightforwardly interpreted as evidence that

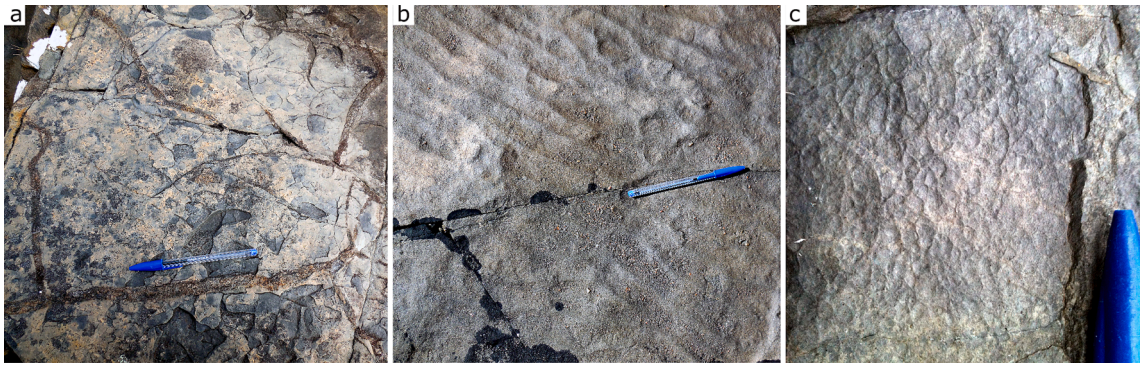

Fig. 2. Features typical of bed surfaces in the mudstone-bearing intervals of the Diabaig and Loch na Dal formations. **(a)** Desiccation cracks. **(b)** Low-amplitude oscillation (wave) ripples; note coarse lags concentrated in troughs of ripples. **(c)** Microbially induced sedimentary structures.

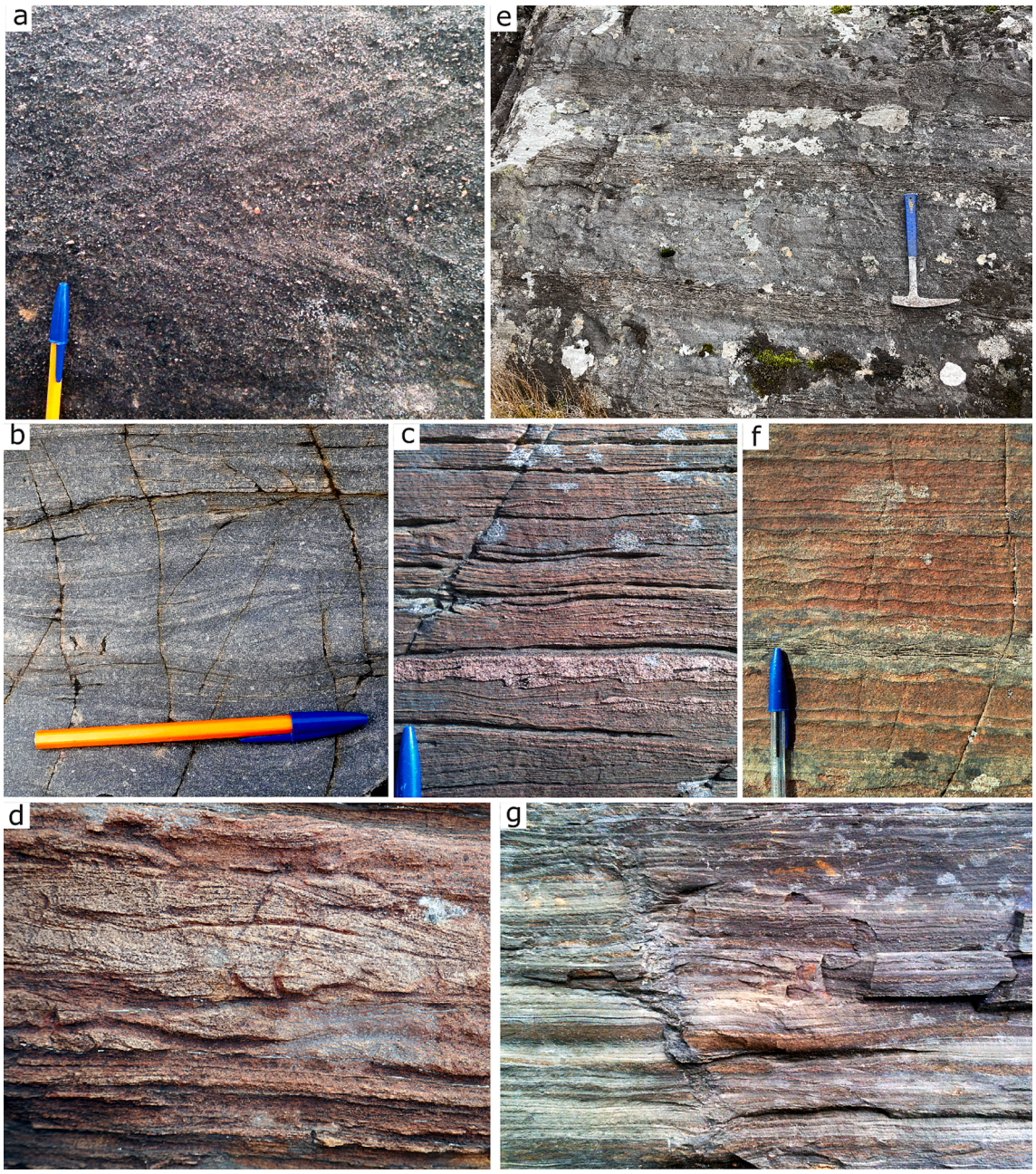

Fig. 3. Tide generated sedimentary features. **(a)** Herringbone cross bedding. **(b, c, d)** Mud-drapes and partings in rippled and wavy-parallel laminated beds with multiple reactivation surfaces. (**e, f, g**). Sets of repetitively alternating sets of thicker-coarser and thinner-finer laminae interpreted as tidal bundles and tidal rhythmites.

sedimentation occurred in mixed-energy, nearshore-marine settings fringed by fluvial networks. The bimodal flow indicators and rippled beds with reactivation surfaces confirm deposition by tidal currents and the repetitively thin-thick laminae in cm- to dm-thick sets can be viewed as tidal bundles and tidal rhythmites. The abundance of desiccation cracks shows that those settings were repeatedly exposed subaerially. The overall fine-grained nature of much of the Diabaig and Loch na Dal sediments together with the preservation on many bed surfaces of microbially induced sedimentary structures (MISS) and low-amplitude wave ripples suggests that deposition of the mudstone-dominated intervals was under relatively low-energy conditions. The rare development of hummocky-swaley stratification and soft-sediment deformation denotes that higher-energy events modified those settings but were infrequent. As per the interpretation of previous workers (e.g. Stewart, 2002 and references therein), the sharp- to scalloped-based to channelled sandstone beds marked by trough cross-bedding yielding unidirectional paleocurrents represent fluvial deposits. The systematic organisation of facies features into vertically stacked depositional cycles implies that depositional environments were laterally adjacent, migrating across one another over time. Thus, sedimentological observations negate a lacustrine origin of the Diabaig and Loch na Dal mudstones. Instead, they imply a shallow water setting flushed by tides, calm enough to enable deposition of mud, and experiencing occasional storms, and that this depositional system was bordered by rivers. We then turned our attention to acquiring geochemical data to inform on salinity and redox conditions.

4.2. *Geochemical evidence of weakly saline, oxic conditions*

In modern sediments, it has been shown that B/Ga, Sr/Ba, and TRS/

Fig. 4. Typical sedimentary motifs across the Diabaig and Loch na Dal outcrop belts. **(a, b, c)** Diabaig Formation, Rum, showing m-scale thickening- and coarsening-upward cycle marked by ball-n-pillow structures implying rapidly emplaced event beds and ripple co-sets showing bimodal flow directions (height of photo c is ~ 20 cm). **(d, e)** Diabaig Formation, Raasay, showing sharp-based trough cross-bedded sandstone sitting sharply on mudstone-dominated interval containing flaser-lenticular-pinstripe bedded ripples showing reversing flow indicators. **(f, g)** Diabaig Formation, Badenscaille, showing flat-based planar-laminated and shallow trough cross-bedded sandstones with mudstone layers marked by flaser-bedded ripples displaying reactivation surfaces, mud drapes and 180°-opposed migration directions. (h, i) Loch na Dal Formation, Type Locality, showing flaser-lenticular-pinstripe bedding occurring in bundles and with ripples displaying abundant mud drapes, reactivation surfaces and compound-ripple geometries (height of photo h is ~ 60 cm).

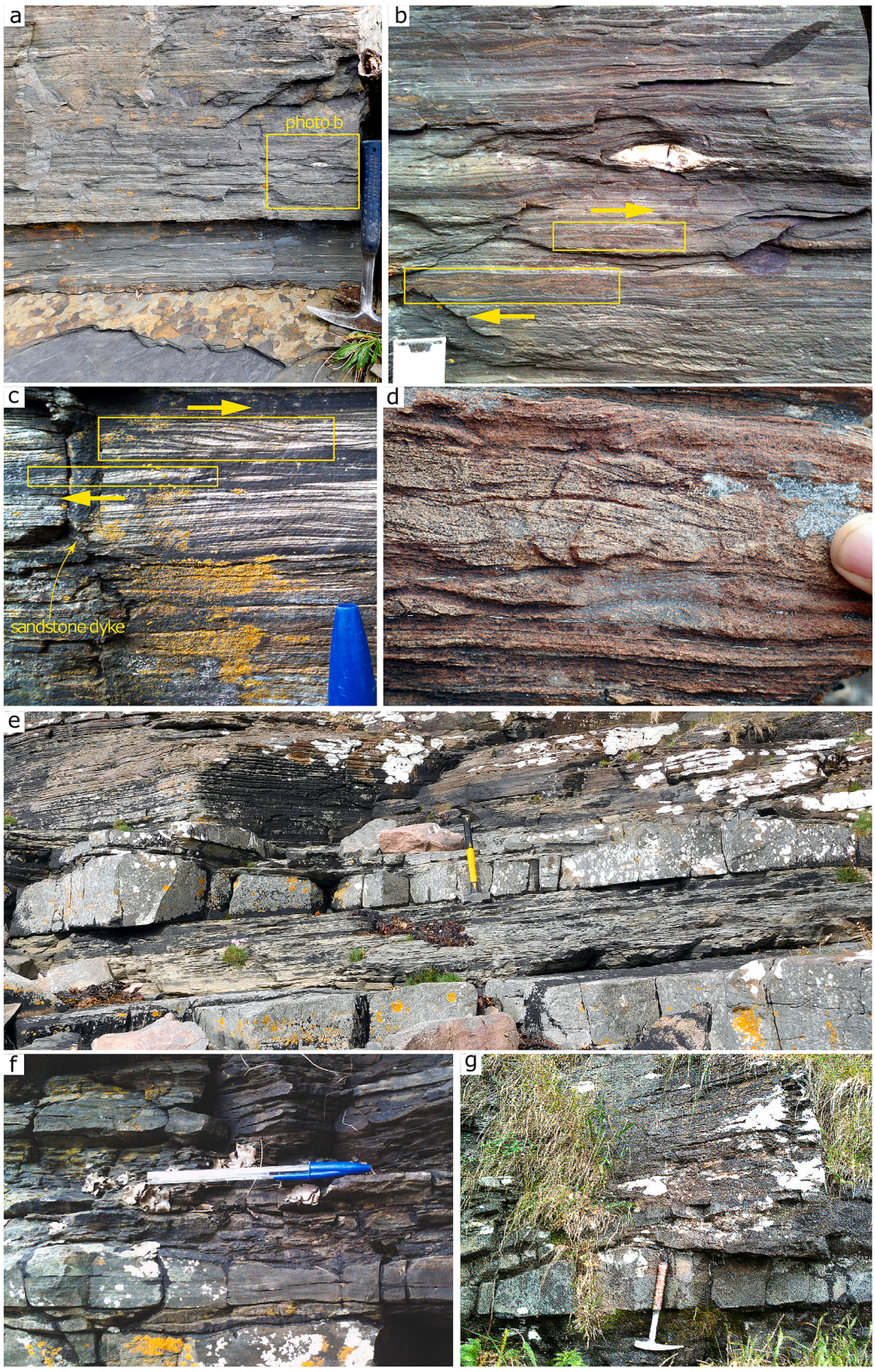

Fig. 5. Tide- and storm-generated sedimentary structures in the Diabaig Formation at the Type Locality. **(a)** Typical grey eukaryote-fossil-bearing mudstone with phosphatic nodules and layers (weathered white). **(b)** Phosphatic nodule occurring encased in mudstones containing starved ripples (i.e. lenticular bedding) showing 180̊-opposed migration directions. **(c)** Ripple trains with mud drapes and reactivation surfaces showing 180̊-opposed migration directions. **(d)** Ripples with multiple reactivation surfaces and mud drapes separated by mud partings. **(e, f, g)** Variably sized hummocky and swaley cross-stratified beds encased in mudstone-dominated intervals.

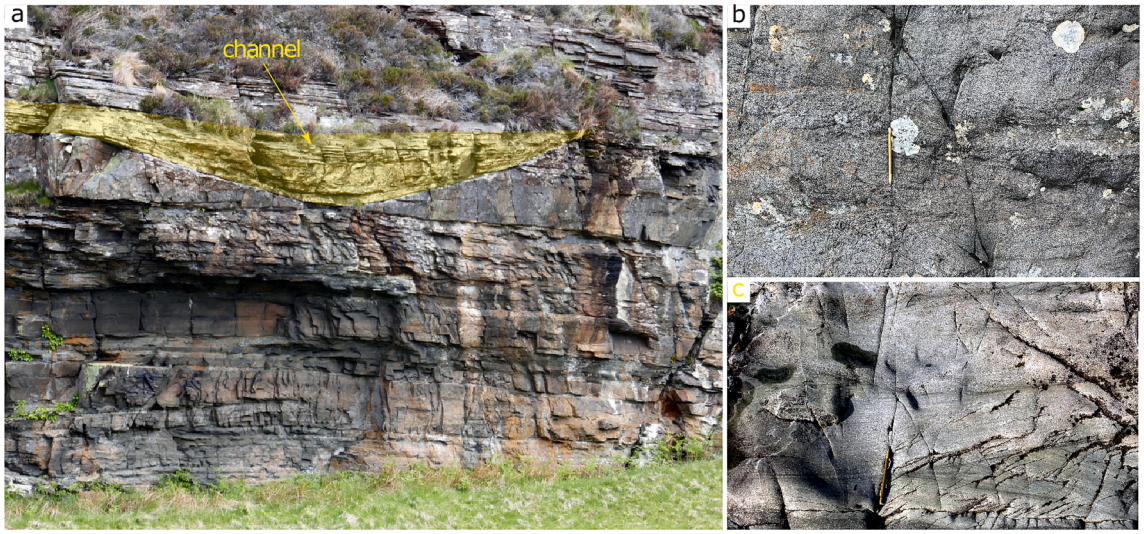

Fig. 6. Fluvial sandstone bodies. **(a)** Channel incised into flat laminated sandstone body (Diabaig Formation, Loch Veyatie). **(b,c)** Nested co-sets of dm-scale trough cross-bedding in medium to coarse-grained quartz-feldspathic sandstone (Diabaig Formation, Rum, and Loch na Dal Formation, Type Locality, respectively).

TOC are proxies for differentiating fresh from brackish from marine waters (Algeo & Ingall, 2007; Wei & Algeo, 2020; Jewuła et al., 2022). The B/Ga proxy is based on the observation that seawater has a higher boron concentration than freshwater while Ga is unaffected by salinity. Both elements adsorb to clay minerals within sediments, however Ga is less reactive than B and the majority of dissolved Ga precipitates out into soils and sediments as hydroxides on its way to marine environments (Wei & Algeo, 2020). At face value, the data obtained for our samples suggest freshwater conditions (Fig. 7b). The Sr/Ba proxy operates on the premise that Ba reacts quickly with marine sulfate while Sr adsorbs to clays such that the Sr/Ba ratio of clay bearing sediments increases with marine influence (Wei & Algeo, 2020). The results for our samples fall in the range of fresh to brackish waters (Fig. 7a) It is uncertain how well the Sr/Ba proxy applies to the Precambrian, and whether the empirically calibrated thresholds apply in the same manner, because the marine Sr and Ba reservoirs may have been significantly impacted by the rise of increasing marine sulfate levels (Fakhraee et al., 2019), increasing seawater pH (Halevy & Bachan, 2017) and possibly other changes in water chemistry associated with the Precambrian-Phanerozoic transition. However, as both Sr/Ba and B/Ga point in the same direction, it is perhaps more likely that the Diabaig and Loch na Dal sediments were deposited in predominantly fresh waters (Fig. 7a,b). We note that the Sr/Ba proxy may be impacted by the presence of carbonate phases in the rock, which may introduce additional Sr beyond the clay-bound component. But in this sample set, carbonate was essentially absent, as also indicated by low Ca abundances, and can therefore be ruled out as a major driver of Sr/Ba ratios.

The TRS/TOC ratio is also a salinity proxy because marine waters usually contain more sulfate than freshwater, meaning higher degrees of sulfate reduction and deposition of sulfide phases in marine sediments (Hedges & Keil, 1995; Togunwa & Abdullah, 2017). This proxy has been applied to Proterozoic successions (Diamond et al., 2018). Our values of 0.01 to 0.46 suggest a mix between freshwater and brackish conditions (Wei & Algeo, 2020). However, TOC levels are low, possibly due to relatively oxic conditions that hindered biomass preservation. Some carbon may also have been lost during low-grade metamorphism. Low primary TOC levels may have slowed down sulfate reduction, making it difficult to distinguish between marine and non-marine conditions based on the TRS/TOC proxy alone. An additional hurdle for this proxy is the potentially low sulfate reservoir of the Proterozoic ocean (Fakhraee et al., 2019). We will revisit this point in the context of sulfur isotopes below.

To shed light on redox conditions, we used C_{org}/P and metal-based proxies, including Mo, Fe/Al, U/Th, Ni/Co and V/Cr. We stress that the transition metal ratios (Ni/Co and V/Cr) have been shown to be unreliable, as all transition metals are redox sensitive to some extent and therefore the ratio's response to redox changes may be subtle or even unpredictable (Algeo & Liu, 2020). An additional confounding factor is the potentially small dissolved reservoir of these elements in freshwater as well as in Proterozoic seawater (Robbins et al., 2016). We nevertheless include these proxies here to not miss any unusual geochemical trends that may be informative about the paleoenvironment. C_{org}/P was chosen as a redox proxy for this dataset because the phosphorous cycle is closely associated with productivity (carbon burial) and the concentration of atmospheric oxygen. This proxy works through a combination of a positive feedback loop on short timescales ($<10^3$ yr), where P fluxes can jumpstart primary production in oxygen-poor depositional environments creating a sink for C_{org}, and a negative feedback loop on longer timescales ($>10^6$ yr), where C_{org} burial causes an increase in atmospheric O_2 (Algeo & Ingall, 2007). Empirical calibration suggests that C_{org}/P values > 100 are indicative of euxinic redox conditions, values of 50–100 indicate suboxic redox conditions, and values < 50 can indicate dysoxic-oxic redox conditions. Our C_{org}/P values range from 0.73 to 10.31, with the exception of a sample from Victoria Falls with a C_{org}/P value of 27.72. These values support an oxic redox environment (Fig. 7d). Mo is typically enriched in marine shales under anoxic conditions because the ocean has a relatively large dissolved Mo reservoir, and Mo becomes particle-reactive in anoxic waters (Scott & Lyons, 2012). The smaller Mo reservoir in freshwater is certainly an impediment to the quantitative framework of this proxy (Scott & Lyons, 2012); however, Mo enrichments have been documented from a modern anoxic freshwater lake (Glass et al., 2013), indicating that Mo abundances can still be informative in non-marine settings. Our samples fall mostly below 1.1 μg/g total Mo, which means that they are depleted relative to average continental crust. Such a depletion may suggest that Mo was mobilised under oxic conditions. Deposition in an anoxic environment appears unlikely. Our results for Fe/Al (0.58 ± 0.05, Fig. 7c) further support this conclusion as they fall within the empirically determined range of oxic settings (Raiswell et al., 2018). The same holds true for U/Th (0.38 ± 0.06), Ni/Co (2.07 ± 0.25, not plotted), and V/Cr (1.60 ± 0.15) ratios (Fig. 7d). As noted above, Ni/Co and V/Cr have been found to be unreliable (Algeo & Liu, 2020), but in our case, the data show no unusual behaviour and likely indicate mobilisation and transport under oxic conditions (e.g., Jones & Manning, 1994; Shaw et al. 1990; Ernst,

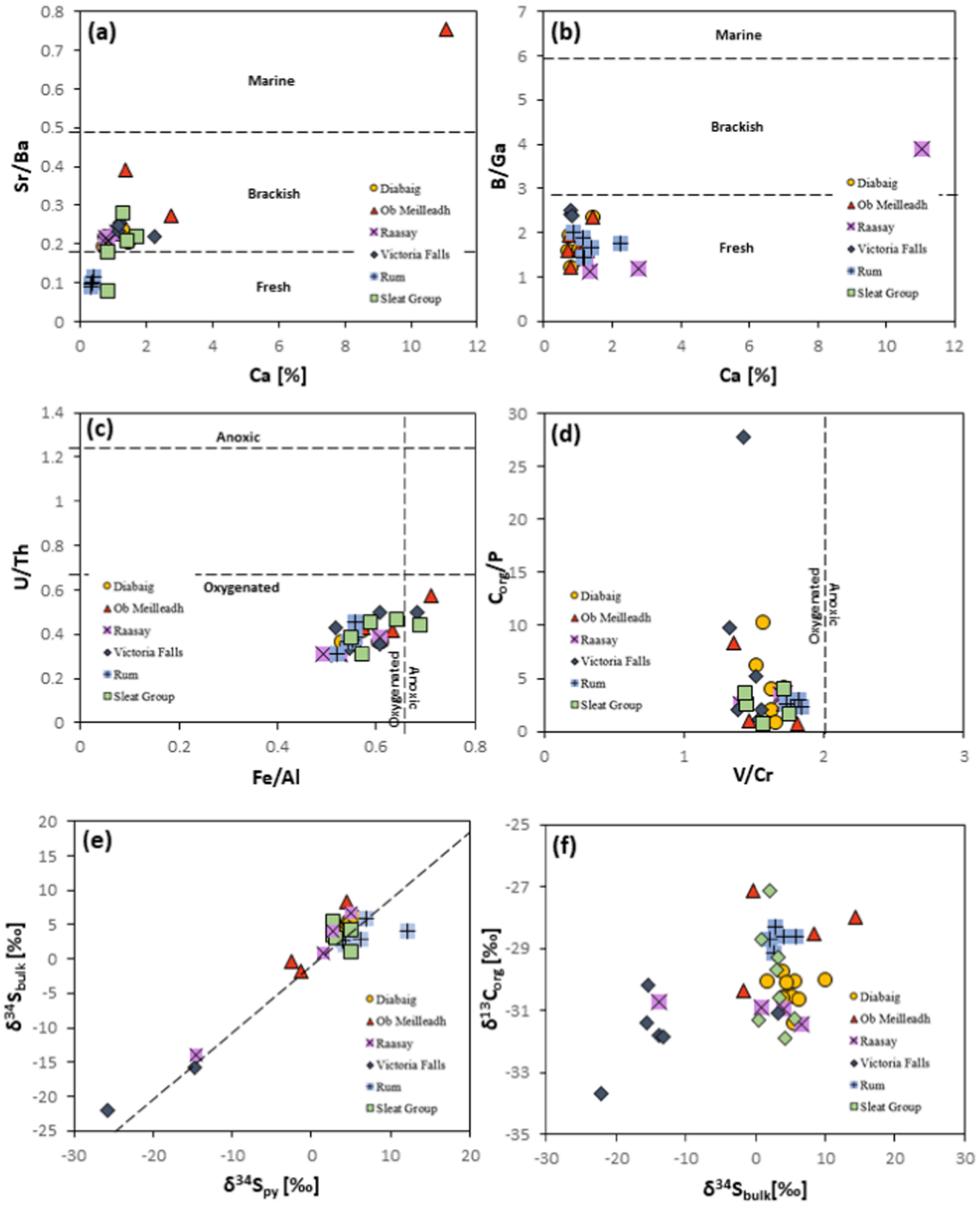

Fig. 7. Geochemical and isotope data plots. Paleosalinity proxies of (a) Sr/Ba and (b) B/Ga shown against percent Ca to test if carbonate has impacted either proxy (B/Ga data for Rum and Loch na Dal rocks was not measured). Redox proxies of (c) Fe/Al (mean 0.58 ± 0.05) plotted against U/Th (mean 0.38 ± 0.06) and (d) C_{org}/P (mean 4.22) plotted against V/Cr (mean value 1.60 ± 0.15). These values plot firmly below thresholds shown by Wei & Algeo (2020), Jones & Manning (1994) and Ernst (2012). (e) $\delta^{34}S_{bulk}$ and $\delta^{34}S_{py}$ and (f) $\delta^{34}S_{bulk}$ and $\delta^{13}C_{org}$ cross plots. The dashed line in panel (e) represents a 1:1 relationship. In panels (a)-(d) the vertical and horizontal dashed lines represent empirically calibrated redox thresholds (see references).

2012). In summary, the fact that none of these proxies show evidence of anoxia leads us to conclude that the Diabaig and Loch na Dal settings were oxygenated.

Regarding the sulfur isotope data, excepting one locality and a few outliers, the $\delta^{34}S_{py\ \&\ bulk}$ values for the Diabaig and Loch na Dal rocks are largely between −2 ‰ to + 9 ‰ (Fig. 7e,f), which is a much narrower spread than found in other mid-Proterozoic marine shales (-35 ‰ to 50 ‰; Shen et al. 2003; Johnston et al., 2008; Gilleaudeau & Kah, 2015; Stüeken et al., 2022). Considering that the Diabaig and Loch na Dal sediments were deposited in an oxic setting, microbial sulfate reduction was likely restricted to porewaters, and one would expect the $\delta^{34}S_{py\ \&\ bulk}$ data to display Rayleigh distillation towards the composition of the sulfate reservoir. Proterozoic marine sulfate had a composition of c. 20–30 ‰ (Luo et al., 2015), much heavier than our samples. Instead, a more compatible sulfate source may have been freshwater (Fig. 8a). If riverine sulfate in the Proterozoic had a composition of c. 6 ‰ (Fike et al., 2015), comparable to the modern value of 4.8 ‰ (Burke et al., 2018), our data would be consistent with nearly quantitative sulfate

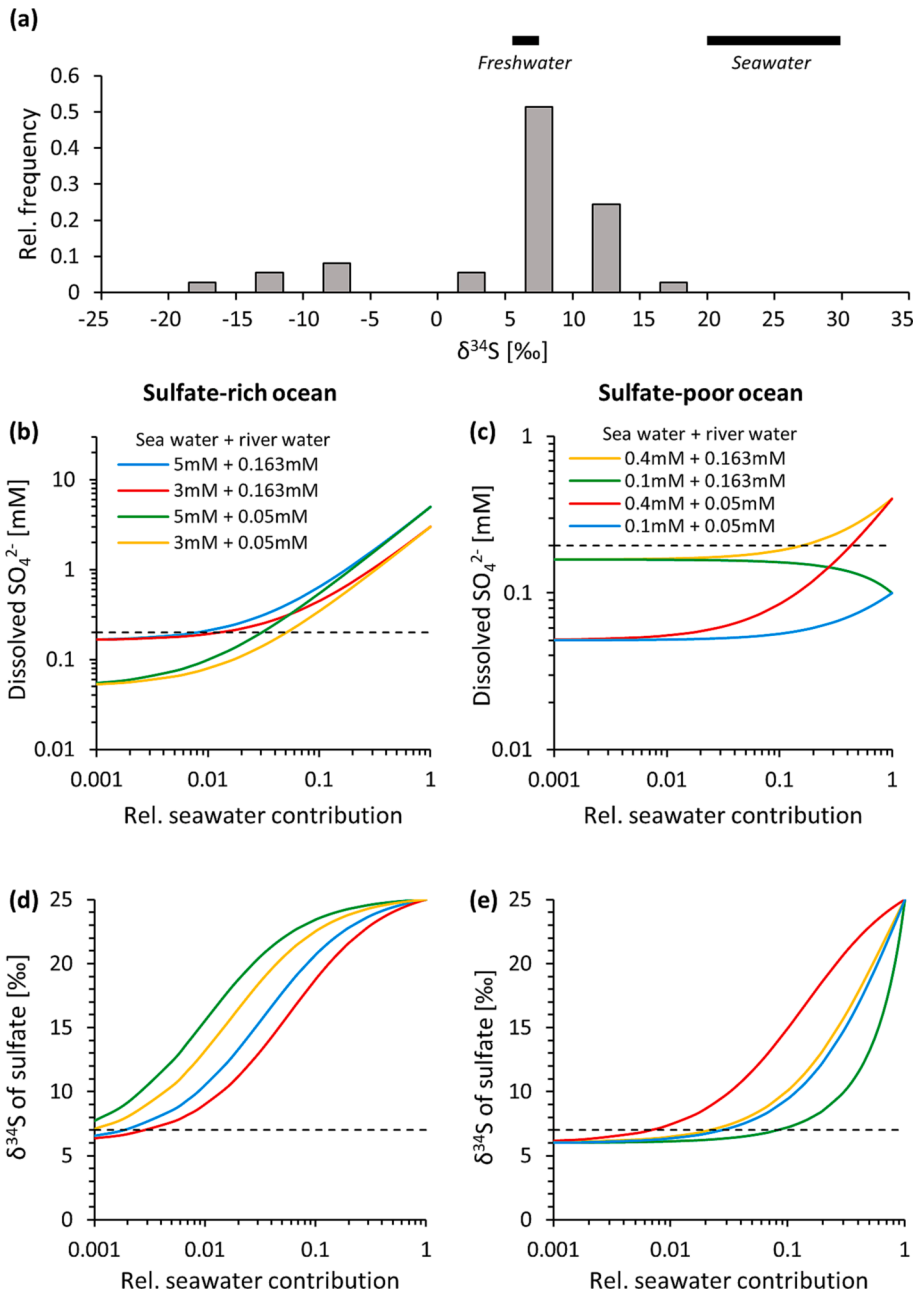

Fig. 8. (a) Histogram of $d^{34}S_{bulk}$ for the Diabaig and Loch na Dal formations compared to typical ranges of freshwater and seawater values. (b-e) Seawater-freshwater mixing calculations. Upper panels show the concentration of sulfate for mixtures from 0.01 to 100 % seawater. Assumed concentrations of sulfate in the two endmembers are shown in the format 'seawater [SO_4^{2-}] + freshwater [SO_4^{2-}]'. Input data are taken from the literature as detailed in the text. (Fike et al., 2015; Luo et al., 2015; Burke et al., 2018; Fakhraee et al., 2019). The dashed line in panel (b) and (c) at 0.2 mM marks the concentration below which microbial sulfate reduction is typically quantitative and does not lead to significant isotopic fractionation (Habicht et al., 2002). Panels (d) and (e) show the corresponding isotopic composition of sulfate. The dashed line at 7 ‰ is the upper limit for most of our samples and could represent the composition of sulphate sulfate in the basin. Panels (b) and (d) apply to a scenario where the ocean was sulfate-rich compared to Proterozoic rivers; panels (c) and (e) are for a sulfate-poor ocean, as suggested by Fakhraee et al. (2019).

reduction of riverine sulfate within pore waters, as documented from modern sulfate-poor lakes (Gomes et al., 2013).

The exception to this is the Victoria Falls locality in the Diabaig Formation, which has lower $\delta^{34}S_{py\ \&\ bulk}$ (Fig. 7e,f), suggesting incomplete sulfate reduction to sulfide. TOC contents at Victoria Falls (median 1852 +1769/-905 μg/g) are statistically not distinguishable ($p_{two\text{-}tailed}$ = 0.18) from the rest of the sample set (Table 1; median 1203 +859/-501 μg/g), indicating that the lower values cannot be explained by lower productivity and a more limited supply of reductants for sulfate reduction. An alternative explanation is that the paleoenvironment at Victoria Falls had a somewhat larger sulfate reservoir. In this case, if the absolute amount of sulfate reduction was equivalent to other localities in the Diabaig Formation (due to similar TOC loadings), more unused sulfate would have remained in the environment, and isotopic fractionations associated with sulfate reduction would have been expressed in the sedimentary sulfide pool. We therefore tentatively interpret these data as indicating a larger marine water input at Victoria Falls compared to the other localities.

4.3. Integrating sedimentology and geochemical proxies

Our geochemical and S-isotope data are most parsimoniously interpreted as evidence of oxygenated fresh water conditions during deposition of the Diabaig and Loch na Dal formations, with the exception of the Victoria Falls locality, where we tentatively infer higher marine sulfate input. In contrast, the sedimentary features of these rocks indicate marine tides and, rarely, storm processes. These seemingly conflicting datasets can be reconciled by interpreting those formations as having been deposited in a setting where tides operated and conditions fluctuated between fresh and saline, i.e., an estuary.

To explore this more quantitatively, we assessed the S-isotope data via simple mixing calculations between plausible end-member scenarios (Fig. 8b–e). The parameters used were: $\delta^{34}S$ of marine sulfate of 25 ‰, two sulfate-rich (3 and 5 mM; Luo et al., 2015) and -poor seawater endmembers (0.1 and 0.4 mM; Fakhraee et al., 2019), postulated isotopic composition of Proterozoic riverine sulfate of 6 ‰ (Fike et al., 2015), the modern average riverine sulfate concentration of 0.163 mM (Burke et al., 2018), and a lower riverine concentration of 0.05 mM (Fakhraee et al., 2019, using their riverine sulfur flux divided by the riverine water flux). The narrow range and overall scarcity of negative $\delta^{34}S$ values in our sample set suggests that microbial sulfate reduction went to completion, which is typically the case if sulfate levels are below 0.2 mM (Habicht et al., 2002; dashed line Fig. 8b,c). This constraint of < 0.2 mM alone could theoretically allow 100 % seawater in the basin if the ocean was sulfate poor. However, if that were the case, we would expect $\delta^{34}S$ values to cluster closer to 25 ‰, i.e., the $\delta^{34}S$ value of Meso-Neoproterozoic oceans (Fike et al., 2015; Luo et al., 2015; Fakhraee et al., 2019), rather than the samples' mode of c. 7 ‰ (dashed line Fig. 8d,e).

Assuming instead that c. 7 ‰ represents the average composition of sulfate in the water column at our sampling sites, and that this sulfate was quantitatively reduced by microbial sulfate reduction within pore waters, the contribution of seawater would have been below 10 %. Put differently, the geochemical data permit a few percent of seawater influx (and possibly more at the Victoria Falls locality), which reconciles those data with sedimentological evidence of tidal push and pull.

4.4. Implications for the early biosphere

Our findings carry broad implications for the emerging view of eukaryogenesis and evolution during the Proterozoic. Eukaryotic microfossils are known back to approximately 1.65 Ga (Fig. 9). Among this record, the Stoer-Sleat-Torridon rocks are one of only two successions thought to archive lacustrine conditions. The other is the Nonesuch Formation of the Midcontinent Rift, USA (Strother & Wellman, 2016, 2020). Our previous geochemical and sedimentological observations for that formation (Jones et al., 2020; Stüeken et al., 2020) and the Poll a'Mhuillt unit of the Stoer Group (Stüeken et al., 2017) show that, rather than lakes, those rocks record estuarine environments with variable amounts of seawater entrainment, although this interpretation is not yet universally accepted (Slotznick et al., 2023). It has been well documented that some of the eukaryotic fossils were transported by rivers and therefore did not live *in situ* within the Torridonian setting (Strother et al., 2011; Strother & Wellman, 2016). Nevertheless, these organisms continue to represent the oldest non-marine eukaryotic organisms. However, in other cases, this is ambiguous, especially in the case of fossils preserved within phosphatic nodules that display exquisite detail that should not have been preserved in the event of river transport. Such *in situ* ecosystems thus must have been living at the interface between freshwater and seawater. Our geochemical data suggest on average lower salinities than inferred for the Nonesuch and Poll a' Mhuilt strata, where a seawater influence is evident from sedimentary features as well as high Mo enrichments and large sulfur isotope fractionations (Stüeken et al., 2017, Jones et al., 2020; Stüeken et al., 2020). Recent phylogenetic work indicates that eukaryotic algae first emerged in low-salinity habitats c. 1.9 Gyr ago (Sanchez-Baracaldo et al. 2017). If so, estuaries may have been that habitat with the additional benefit that they perhaps facilitated the transition towards the marine realm.

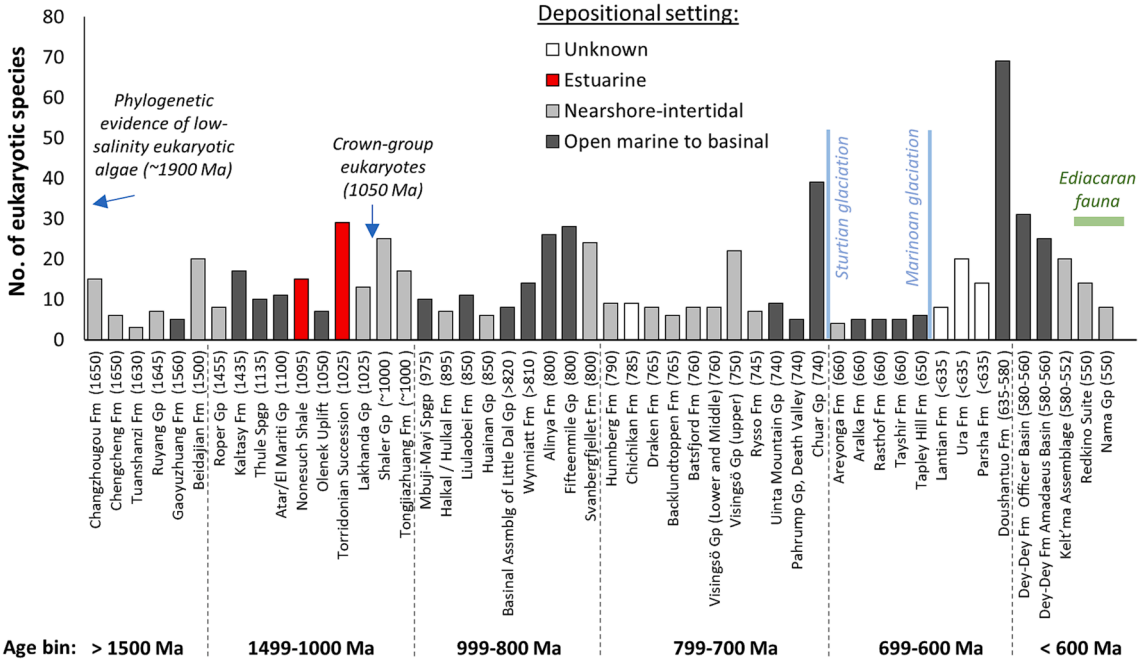

Fig. 9. Diversity of eukaryotic microfossils through Proterozoic time (ages shown in Ma). Data and associated references are taken from the compilation by Lyons et al. (2021) modified using data from Strother et al. (2011) and Slotznick et al. (2023)for the Torridonian and Nonesuch compilations, respectively. Depositional settings for each formation are taken from the original source data, cited by Lyons et al. (2021). The date for phylogenetic evidence for the emergence of eukaryotic algae adapted to low salinities is taken from Sánchez-Baracaldo et al. (2021). Marked in red are two stratigraphic units that were previously classed as fully non-marine and have recently revealed evidence of tidal seawater influx, akin to estuarine settings (Jones et al., 2020; Stüeken et al., 2020; this study).

5. Conclusions

The Diabaig and Loch na Dal formations in northwest Scotland are renowned for their organic-walled microfossils considered to be some of the oldest known non-marine eukaryotic biotas. As demonstrated by careful paleontological work, many of these fossils were likely transported and did not necessarily live within the environment in which they were found (Strother et al., 2011; Strother & Wellman, 2016). Traditionally, the eukaryotic-bearing rocks were thought to be lacustrine (Stewart, 2002 and references therein); however, our new sedimentological observations combined with new geochemical data from 40 samples of grey mudstones show that interpretation is incorrect. The presence of wave-, tide- and storm-current-generated sedimentary structures (e.g., herringbone cross-strata, flaser-lenticular-pinstripe bedding, hummocky stratification) indicate that deposition occurred in marine-influenced settings. Salinity estimates based on sulfur isotopes, Sr/Ba, B/Ga and TRS/TOC ratios imply mostly fresh waters with perhaps just a few percent seawater input while redox proxies of Mo concentrations, Fe/Al, C_{org}/P, U/Th, Ni/Co and V/Cr ratios indicate oxic conditions. An environmental setting compatible with both the geochemical data and sedimentology is an estuary where tides and mixing fronts between freshwater discharges and marine incursions are common. Similar findings for the eukaryotic-bearing Poll a'Mhuillt Member in NW Scotland (Stüeken et al., 2017) and the c. 1.1 Ga Nonesuch Formation of the Midcontinent Rift USA (Jones et al., 2020; Stüeken et al., 2017), show that they, too, were deposited in estuarine-like settings. Consequently, our findings indicate that those organisms that lived *in situ* in these late Stenian–early Tonian basins were likely exposed to frequently changing water conditions. These gradients in water chemistry over space and time may have facilitated the transition of eukaryotes from freshwater to the marine realm (Sánchez-Baracaldo et al., 2017).

CRediT authorship contribution statement

Grace C. Nielson: Writing – review & editing, Writing – original draft, Project administration, Data curation, Conceptualization. **Eva E. Stüeken:** Writing – review & editing, Supervision, Resources, Project administration, Methodology, Formal analysis, Data curation, Conceptualization. **Anthony R. Prave:** Writing – review & editing, Supervision, Resources, Project administration, Methodology, Conceptualization.

Declaration of competing interest

The authors declare that they have no known competing financial interests or personal relationships that could have appeared to influence the work reported in this paper.

Data availability

All data generated in this study are presented in Tables 1 and 2.

Acknowledgements

We thank Tom Algeo and the other reviewers, who wished to remain anonymous, for detailed and productive feedback that improved our manuscript. We thank Frances Westall for efficient editorial handling. EES acknowledges financial support from a NERC Frontiers grant (NE/V010824/1).

References

Algeo, T.J., Ingall, E., 2007. Sedimentary Corg: P ratios, paleocean ventilation, and Phanerozoic atmospheric pO2. Palaeogeogr. Palaeoclimatol. Palaeoecol. 256 (3–4), 130–155.
Algeo, T.J., Liu, J., 2020. A re-assessment of elemental proxies for paleoredox analysis. Chem. Geol. 540, 119549.
Brasier, A.T., Culwick, T., Battison, L., Callow, R.H.T., Brasier, M.D., 2017. Evaluating evidence from the Torridonian Supergroup (Scotland, UK) for eukaryotic life on land in the Proterozoic. Geol. Soc. Lond. Spec. Publ. 448 (1), 121–144.
Burke, A., Present, T.M., Paris, G., Rae, E.C.M., Sandilands, B.H., Gaillardet, J., Peucker-Ehrenbrink, B., Fischer, W.W., McClelland, J.W., Spencer, R.G., Voss, B.M., 2018. Sulfur isotopes in rivers: Insights into global weathering budgets, pyrite oxidation, and the modern sulfur cycle. Earth Planet. Sci. Lett. 496, 168–177.
Callow, R.H., Battison, L., Brasier, M.D., 2011. Diverse microbially induced sedimentary structures from 1 Ga lakes of the Diabaig Formation, Torridon Group, northwest Scotland. Sed. Geol. 239 (3–4), 117–128.
Canfield, D.E., Raiswell, R., Westrich, J.T., Reaves, C.M., Berner, R.A., 1986. The use of chromium reduction in the analysis of reduced inorganic sulfur in sediments and shales. Chem. Geol. 54 (1–2), 149–155.
Diamond, C.W., Planavsky, N.J., Wang, C., Lyons, T.W., 2018. What the~ 1.4 Ga Xiamaling Formation can and cannot tell us about the mid-Proterozoic ocean. Geobiology 16 (3), 219–236.
Ernst, W. 2012. *Geochemical facies analysis*. Elsevier, pp 158.
Fakhraee, M., Hancisse, O., Canfield, D.E., Crowe, S.A., Katsev, S., 2019. Proterozoic seawater sulfate scarcity and the evolution of ocean–atmosphere chemistry. Nat. Geosci. 12 (5), 375–380.
Fike, D.A., Bradley, A.S., Rose, C.V., 2015. Rethinking the ancient sulfur cycle. Annu. Rev. Earth Planet. Sci. 43, 593–622.
Gilleaudeau, G.J., Kah, L.C., 2015. Heterogeneous redox conditions and a shallow chemocline in the Mesoproterozoic ocean: Evidence from carbon-sulfur-iron relationships. Precambr. Res. 257, 94–108.
Glass, J.B., Chappaz, A., Eustis, B., Heyvaert, A.C., Waetjen, D.P., Hartnett, H.E., Anbar, A.D., 2013. Molybdenum geochemistry in a seasonally dysoxic Mo-limited lacustrine ecosystem. Geochim. Cosmochim. Acta 114, 204–219.
Gomes, M.L., Hurtgen, M.T., 2013. Sulfur isotope systematics of a euxinic, low-sulfate lake: Evaluating the importance of the reservoir effect in modern and ancient oceans. Geology 41 (6), 663–666.
Habicht, K.S., Gade, M., Thamdrup, B., Berg, P., Canfield, D.E., 2002. Calibration of sulfate levels in the Archean ocean. Science 298 (5602), 2372–2374.
Halevy, I., Bachan, A., 2017. The geologic history of seawater pH. Science 355 (6329), 1069–1071.
Hedges, J.I., Keil, R.G., 1995. Sedimentary organic matter preservation: an assessment and speculative synthesis. Mar. Chem. 49 (2–3), 81–115.
Ielpi, A., Ghinassi, M., 2015. Planview style and palaeodrainage of Torridonian channel belts: Applecross Formation, Stoer Peninsula, Scotland. Sed. Geol. 325, 1–16.
Jewuła, K., Środoń, J., Kędzior, A., Paszkowski, M., Liivamägi, S., Goryl, M., 2022. Sedimentary, climatic, and provenance controls of mineral and chemical composition of the Ediacaran and Cambrian mudstones from the East European Craton. Precambr. Res. 381, 106850.
Johnston, D.T., Farquhar, J., Summons, R.E., Shen, Y., Kaufman, A.J., Masterson, A.L., Canfield, D.E., 2008. Sulfur isotope biogeochemistry of the Proterozoic McArthur Basin. Geochim. Cosmochim. Acta 72 (17), 4278–4290.
Jones, B., Manning, D.A., 1994. Comparison of geochemical indices used for the interpretation of palaeoredox conditions in ancient mudstones. Chem. Geol. 111 (1–4), 111–129.
Jones, S.M., Prave, A.R., Raub, T.D., Cloutier, J., Stüeken, E.E., Rose, C.V., Linnekogel, S., Nazarov, K., 2020. A marine origin for the late Mesoproterozoic Copper Harbor and Nonesuch Formations of the Midcontinent Rift of Laurentia. Precambr. Res. 336, 105510.
Krabbendam, M., Strachan, R., Prave, T., 2022. A new stratigraphic framework for the early Neoproterozoic successions of Scotland. J. Geol. Soc. London 179 (2) jgs2021-054.
Luo, G., Ono, S., Huang, J., Algeo, T.J., Li, C., Zhou, L., Robinson, A., Lyons, T.W., Xie, S., 2015. Decline in oceanic sulfate levels during the early Mesoproterozoic. Precambr. Res. 258, 36–47.
Lyons, T.W., Diamond, C.W., Planavsky, N.J., Reinhard, C.T., Li, C., 2021. Oxygenation, life, and the planetary system during Earth's middle history: An overview. Astrobiology 21 (8), 906–923.
McMahon, W.J., Davies, N.S., 2020. Physical and biological functioning in Proterozoic rivers: evidence from the archetypal pre-vegetation alluvium of the Torridon Group, NW Scotland. Scott. J. Geol. 56, 1–29.
Prave, A.R., 2002. Life on land in the Proterozoic: Evidence from the Torridonian rocks of northwest Scotland. Geology 30, 811–814.
Raiswell, R., Hardisty, D.S., Lyons, T.W., Canfield, D.E., Owens, J.D., Planavsky, N.J., Poulton, S.W., Reinhard, C.T., 2018. The iron paleoredox proxies: A guide to the pitfalls, problems and proper practice. Am. J. Sci. 318 (5), 491–526.
Robbins, L.J., Lalonde, S.V., Planavsky, N.J., Partin, C.A., Reinhard, C.T., Kendall, B., Scott, C., Hardisty, D.S., Gill, B.C., Alessi, D.S., Dupont, C.L., Saito, M.A., Crowe, S. A., Poulton, S.W., Bekker, A., Lyons, T.W., Konhauser, K.O., 2016. Trace elements at the intersection of marine biological and geochemical evolution. Earth Sci. Rev. 163, 323–348.
Scott, C., Lyons, T.W., 2012. Contrasting molybdenum cycling and isotopic properties in euxinic versus non-euxinic sediments and sedimentary rocks: Refining the paleoproxies. Chem. Geol. 324, 19–27.
Shaw, T.J., Gieskes, J.M., Jahnke, R.A., 1990. Early diagenesis in differing depositional environments: the response of transition metals in pore water. Geochim. Cosmochim. Acta 54 (5), 1233–1246.
Slotznick, S.P., Swanson-Hysell, N.L., Zhang, Y., Clayton, K.E., Wellman, C.H., Tosca, N. J., Strother, P.K., 2023. Reconstructing the paleoenvironment of an oxygenated Mesoproterozoic shoreline and its record of life. Geol. Soc. Am. Bull.
Stewart, A.D., Craig, G.Y., 1991. Torridonian. Geology of Scotland 65–85.

Stewart, A.D., Parker, A., 1979. Palaeosalinity and environmental interpretation of red beds from the late Precambrian ('Torridonian') of Scotland. Sed. Geol. 22 (3–4), 229–241.
Stewart, A.D., 1988. The Sleat and Torridon Groups. In: Winchester, J.A. (Ed.), Later Proterozoic Stratigraphy of the Northern Atlantic Regions. Springer US, Boston, MA, pp. 104–112.
Stewart, A.D., 2002. The later Proterozoic Torridonian rocks of Scotland: their sedimentology, geochemistry and origin. *Geological Society of London*. Memoir 24, 136 pp.
Strother, P.K., Wellman, C.H., 2016. Palaeoecology of a billion-year-old non-marine cyanobacterium from the Torridon Group and Nonesuch Formation. Palaeontology 59 (1), 89–108.
Strother, P.K., Wellman, C.H., 2021. The Nonesuch Formation Lagerstätte: a rare window into freshwater life one billion years ago. J. Geol. Soc. London 178 (2) jgs2020-133.
Strother, P.K., Battison, L., Brasier, M.D., Wellman, C.H., 2011. Earth's earliest non-marine eukaryotes. Nature 473 (7348), 505–509.
Stüeken, E.E., Bellefroid, E., Prave, A.R., Asael, D., Planavsky, N., Lyons, T., 2017. Not so non-marine? Revisiting the Stoer Group and the Mesoproterozoic biosphere. Geochemical Perspectives Letters 3, 221–229.
Stüeken, E.E., Jones, S., Raub, T.D., Prave, A.R., Rose, C.V., Linnekogel, S., Cloutier, J., 2020. Geochemical fingerprints of seawater in the Late Mesoproterozoic Midcontinent Rift, North America: Life at the marine-land divide. Chem. Geol. 553, 119812.
Stüeken, E.E., Viehmann, S., Hohl, S.V., 2022. Contrasting nutrient availability between marine and brackish waters in the late Mesoproterozoic: Evidence from the Paranoá Group. Brazil. *Geobiology* 20 (2), 159–174.
Sánchez-Baracaldo, P., Raven, J.A., Pisani, D., Knoll, A.H., 2017. Early photosynthetic eukaryotes inhabited low-salinity habitats. Proc. Natl. Acad. Sci. 114 (37), E7737.
Togunwa, O.S., Abdullah, W.H., 2017. Geochemical characterization of Neogene sediments from onshore West Baram Delta Province, Sarawak: paleoenvironment, source input and thermal maturity. Open Geosciences 9 (1), 302–313.
Wei, W., Algeo, T.J., 2020. Elemental proxies for paleosalinity analysis of ancient shales and mudrocks. Geochim. Cosmochim. Acta 287, 341–366.
Wellman, C.H., Strother, P.K., 2015. The terrestrial biota prior to the origin of land plants (embryophytes): a review of the evidence. Palaeontology 58 (4), 601–627.